Full Length Article

# Hollow silica nanospheres with a high content of sorbed molecular hydrogen

Vadim S. Efimchenko [*] , Konstantin P. Meletov , Mariya A. Korotkova , Vladimir M. Masalov ,
Nadezhda S. Sukhinina , Gennadi A. Emel'chenko , Radion I. Usmanov

*Institute of Solid State Physics, Russian Academy of Sciences, Chernogolovka, Moscow District, 2 Academician Ossipyan str. 142432, Russia*

A B S T R A C T

Prospective materials for hydrogen storage should have a high hydrogen content, high adsorption/desorption rates, and consist of abundant elements. Simultaneous implementation of these properties in one material poses a great challenge for researchers. To solve this problem, placement of hydrogen in hollow silicate glass microspheres with a diameter greater than 5 μm was previously proposed as one of the possible ways for hydrogen storage. Additionally, various deuterium-containing spheres were proposed as fuel targets in laser-initiated thermonuclear reactions. In this study, opal matrices consisting of hollow silica nanospheres with an outer diameter of 289 nm and a shell thickness of 25 nm were hydrogenated to X = 0.94 mol $H_2$ per mole $SiO_2$ at a pressure of 7.5 GPa and a temperature of 413 K. This highest hydrogen content of silicates achieved to date dropped to X = 0.8 after keeping the sample in liquid nitrogen at ambient pressure for three days, and then stopped changing. Scanning electron microscopy showed that hydrogenation did not damage the shape of the nanospheres. Raman spectroscopy demonstrated that hydrogen molecules formed a gas in the cavities inside the spherical $SiO_2$ shells and a solid solution in the shells. The density of the hydrogen gas inside the cavities estimated from the intensity of the $H_2$ vibrational mode was about 0.016 g/cm³, which is 52 times greater than its density at the same temperature and normal pressure.

## 1. Introduction

Hydrogen is one of the most promising substances for green energy since its combustion does not lead to the formation of such a greenhouse gas as carbon dioxide. In addition, hydrogen isotopes deuterium and tritium are considered to be the main components of fuel for controlled thermonuclear fusion. However, in all cases, the key problem for the use of hydrogen is its "packaging" in the maximum possible quantity in the minimum volume and mass of the container material. Among the numerous materials and methods for hydrogen storage, such as various metal hydrides [1], complex hydrides decomposed by hydrolysis [2,3], adsorption [4,5], and liquefaction [6] techniques, the accommodation of hydrogen gas in hollow spheres can be identified as a separate category. For example, the accommodation of hydrogen in hollow silicate glass microspheres was previously proposed as one of the possible options for hydrogen storage [7]. Hollow spheres consisting of shells that can be made of various compounds and a deuterium–tritium mixture embedded in the voids were also proposed as fuel targets in laser-

initiated thermonuclear reactions [8]. However, in both cases, the material should correspond to the necessary parameters for its use. To use it for hydrogen storage, it must have sufficient energy capacity per unit mass and volume of the substance [9]. To use spheres filled with deuterium as fuel targets for thermonuclear fusion, it is necessary that (1) the shell material is amorphous; (2) the size of irregularities on the sphere surface does not exceed 1 % of the diameter of the sphere; (3) deuterium embedded in them has a fine crystalline or amorphous form and is uniformly distributed over the inner surface of the sphere [8]. These criteria are necessary to create a centripetal spherically symmetric shock wave that ignites a thermonuclear reaction [10]. The lack of sufficient homogeneity and isotropy in the shell material can break this symmetry and, hence, prevent a thermonuclear reaction. The requirements for the surface of the two-shell targets are not so strict. However, in this case, they must withstand a pressure of 1000–1500 atm since a deuterium–tritium mixture can be used in the gas form [8].

According to the data of [11], a uniform distribution of deuterium over the sphere surface is best achieved when its density inside the

---

sphere is close to or equal to the critical value. Such a density may be created inside the sphere only by introducing hydrogen into the cavity at pressures greater than normal one. Creating smooth spherical fuel targets of the same size is an equally difficult challenge, the implementation of which depends on the material and techniques used. It was proposed to use organic compounds such as polystyrene, lavsan, and polyethylene, as well as inorganic silicate glasses to create such targets. Organic compounds in their initial chemical composition already contain significant amounts of hydrogen. At the same time, silicate spheres have greater strength and, accordingly, are able to accommodate larger amounts of hydrogen gas in their cavities. However, one of the main problems is the uniformity of the shell material and/or a large variation in the sphere size. For example, the diameter of silicate spheres obtained by spraying a gel can differ by several times, as it was shown by Shelby [12]. The sol–gel method allows one to create opal matrices consisting of identical silica particles, the sizes and structure of which depend on the synthesis conditions. It is also possible to form identical hollow $SiO_2$ particles with a diameter of 300 nm and a shell thickness of 30 nm [13,14]. The diameter of these hollow spheres differs by no more than 4 %. In addition, amorphous silica can dissolve up to 0.7 mol of hydrogen per mole of $SiO_2$ and retain it for several years at normal pressure and a temperature of 77 K [15]. Thus, amorphous silica can be saturated with hydrogen to values comparable to hydrogen content in such organic materials as polystyrene, lavsan, and polyethylene.

In recent work [16], we have shown that opal matrices consisting of silicon dioxide particles with a specific surface area of 300–630 m$^2$/g can accommodate X = 0.8 mol of molecular hydrogen per mole of $SiO_2$ after saturation at a pressure of 7.5 GPa and a temperature of 413 K. A significant part of the dissolved hydrogen is introduced not only into the interatomic cavities of $SiO_2$, as in bulk silica glass [9], but also in a gaseous form into the nanocavities formed by silica particles. According to the decomposition data obtained by Raman studies, this amount of dissolved hydrogen decreases by half in 16 years at normal pressure and a temperature of 77 K. Considering that a significant part of hydrogen dissolved in opal structures has a gaseous form, we assume that $H_2$ gas can also penetrate and be retained inside hollow $SiO_2$ spheres under similar conditions. However, there is a possibility of their destruction at both an increase in the pressure up to 7.5 GPa and a decrease in the pressure due to the difference in the external and internal pressure on the sphere, which can arise due to insufficient diffusion of hydrogen through the shell.

In the present paper, we studied the possibility of introducing hydrogen into hollow silica nanospheres at a pressure of P = 7.5 GPa and its subsequent retention at ambient pressure. Opal matrices consisting of hollow silica nanospheres with a diameter of 289 nm were saturated with hydrogen at P = 7.5 GPa and T = 413 K. The hydrogenated samples were quenched to liquid nitrogen temperature, followed by pressure reduction to ambient pressure, and stored at this temperature and normal pressure. The samples were heated above this temperature only to study the hydrogen content and thermal stability by desorption in a pre-evacuated volume. The states of hydrogen and the opal matrix in the hydrogenated samples were studied by Raman spectroscopy at normal pressure and a temperature of 80 K. The integrity and changes in the shape of the nanospheres after their hydrogenation and dehydrogenation were studied using scanning electron microscopy.

## 2. Experimental methods

Hollow silica particles were prepared using the template method. Monodisperse spherical particles of polymethyl methacrylate (PMMA) ~ 300 nm in diameter were synthesized using the emulsion method and served as templates. On the surface of the templates, silicon dioxide shells were formed by the hydrolysis of vinyltrimethoxysilane (VTMS) in an aqueous ammonia solution (0.8 M NH$_3$). After air drying at 60 °C, the hybrid particles were annealed for 3 h at 750 °C. The size and morphology of the particles were monitored using scanning electron

microscopy (a Zeiss Supra 50 VP microscope) and high-resolution transmission-electron microscopy (JEM-2100 microscope). A transmission-electron microscopy image of the initial sample of hollow silica particles is shown in Fig. S1 (Supplementary material). Based on data obtained by the scanning electron microscopy (Fig. S2, Supplementary material), the $SiO_2$ spheres had an average outer diameter of 289 ± 10 nm. The thickness of the shells was estimated to be ~ 25 nm in accordance with [17].

Elemental X-ray microanalysis of the samples revealed the presence of only two chemical elements: 67.2 at.% O and 32.8 at.% Si. In agreement with the previous study [17], X-ray diffraction showed that the samples contained only the amorphous silica phase. The Raman spectrum of the initial sample shown in Fig. 1 almost coincided with the spectrum of silica glass prepared by quenching, which confirmed the amorphous state of the shells of the silica nanospheres.

The hollow silica nanospheres were hydrogenated in a toroid-type high-pressure apparatus [18]. Hydrogen in the reaction cell is obtained by thermal decomposition of the chemical compound $NH_3BH_3$ [19]. The cell is made of Teflon; the sample is separated from $NH_3BH_3$ by Pd foil. The pellet of the opal sample placed into the high-pressure cell had a diameter of ~ 5 mm and a height of ~ 2.5 mm. To ensure the decomposition of $NH_3BH_3$ and hydrogenation of the sample, the temperature and pressure in the cell were varied along the routes indicated in Fig. 2. The pressure was increased in steps of 0.09 GPa per 4 min.

The high-pressure treatment of the samples began with their compression to 1.5 GPa under quasi-hydrostatic conditions, so that the $H_2$ gas released from the aminoborane $NH_3BH_3$ at higher pressure was dense and occupied a sufficiently small volume. Aminoborane decomposes in several stages at temperatures of 400–553 K and eventually forms a binary mixture of gaseous $H_2$ and solid BN [20,21]. In our experiments, it was decomposed at P = 1.5–2 GPa by heating to T = 553 K. Then, the temperature was lowered to T = 413 K, the hydrogen pressure was increased to P = 7.5 GPa, and the samples were kept under these conditions for 30 min. After this procedure, the samples were quenched to liquid nitrogen temperature to exclude hydrogen losses under the subsequent release of pressure to the normal one. The samples were stored in a Dewar vessel with liquid nitrogen. The molar ratio X = $H_2$/$SiO_2$ of the obtained samples was determined with an accuracy of ~ 3 % by hot extraction of the absorbed hydrogen into a pre-evacuated silica glass ampoule [22]. The sample was placed from a liquid nitrogen bath
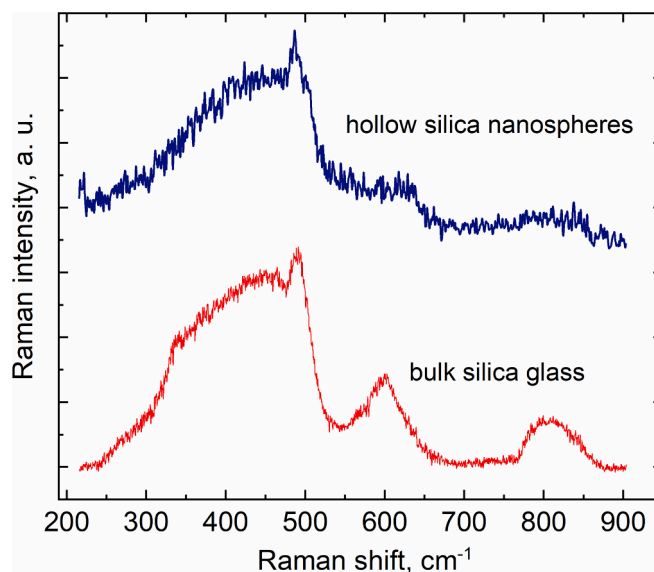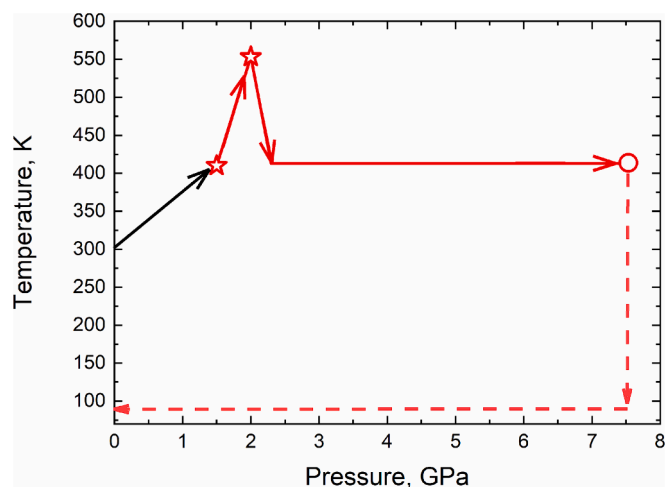


**Fig. 1.** Raman spectra of the sample consisting of hollow silica nanospheres (upper curve) and a sample of bulk silica glass (bottom curve). Both spectra were collected under normal conditions.

**Fig. 2.** Temperature-baric routes of hydrogenation of the opal nanospheres and final cooling (quenching) of the hydrogenated samples. The black and red solid arrows indicate the changes in pressure and temperature under quasi-hydrostatic conditions and in a hydrogen atmosphere, respectively. The asterisks show the decomposition range of the $NH_3 BH_3$ compound used to fill the high-pressure cell with an $H_2$ gas. The open circle shows the pressure and temperature at which the sample was kept for 30 min. The dashed arrows indicate the routes of the sample quenching. (For interpretation of the references to colour in this figure legend, the reader is referred to the web version of this article.)

into an open copper container, while the latter was placed into the quartz ampoule that was cooled from outside by liquid nitrogen. The ampoule was attached to a vacuum system with the calibrated volume, the system was pumped out to 0.136 Pa, and then the ampoule was heated at a rate of 20 K/min with simultaneous measurement of the pressure of the gas released during heating to 873 K. The sample mass was determined by weighing after the measurements, while the mass of the extracted hydrogen was calculated using the data on the ampoule volume and gas pressure.

The Raman spectra were recorded in the back-scattering geometry in the spectral range of 150–4400 $cm^{-1}$ using a setup comprised of an Acton SpectraPro-2500i spectrograph and a CCD Pixis2K detector cooled down to 203 K. A stabilized single-mode YAG laser of 532 nm with an intensity of ∼ 6 mW was focused on the sample in a ∼ 2 μm spot by a × 50 objective of an Olympus BX51 microscope. The spectral resolution was ∼ 3 $cm^{-1}$, and an edge filter with a bandwidth of ∼ 60 $cm^{-1}$

and OD6 suppressed the laser radiation line. The Raman spectra were measured at ∼ 80 K using a homemade nitrogen cryostat allowing cold loading of samples.

## 3. Results and discussion

Fig. 3a shows the thermal desorption curve of the hollow nanospheres measured during the first 4 h after their saturation with hydrogen at a pressure of 7.5 GPa and a temperature of 413 K. The total hydrogen content of the sample X = 0.94 significantly exceeds the previously obtained values of hydrogen solubility in the bulk silica glass (X = 0.6) and the OM1600 opal matrix (X = 0.8) [15,16]. Hydrogen evolution from the nanospheres began at temperatures above 77 K and continued up to 273 K, similar to the hydrogenated OM1600 opal matrices [16]. The amount of dissolved hydrogen in the hollow silica nanospheres decreased to X = 0.8 within five days and did not change thereafter under further storage in liquid nitrogen (Fig. 3 b).

Fig. 4 shows SEM images of the surface of the initial sample before its hydrogenation (a) and after the hydrogenation/dehydrogenation procedures (b). Comparison of the images shows that the spheres retained their original shape despite the initial exposure to a quasi-hydrostatic pressure of 1.5 GPa and subsequent exposures to a hydrogen pressure of 7.5 GPa during the hydrogenation and to temperatures up to 823 K during the dehydrogenation. In addition, unlike the initial sample, the spheres on the surface of the sample subjected to the hydrogenation/dehydrogenation procedure are orderly arranged and close-packed. A possible explanation for their ordering is the action of external pressure before the formation of the hydrogen atmosphere at P = 1.5 GPa.

Fig. 5 depicts a typical Raman spectrum of hydrogen-saturated hollow silica nanospheres measured at 80 K and ambient pressure and, for comparison, a spectrum of the hydrogen-saturated OM1600 opal matrices [16]. In the low-energy part of the spectra, there are broad bands corresponding to silica glass and intense peaks at frequencies of 353 and 587 $cm^{-1}$ corresponding to the rotational modes of free ortho- and parahydrogen molecules [23]. The complex band in the frequency range of 4140–4170 $cm^{-1}$ corresponds to the stretching H-H vibrations of the hydrogen molecules dissolved in the silica shell, as well as of free $H_2$ gas located inside the hollow silica nanospheres. No lines corresponding to Si-H, Si-OH bonds were observed in any spectrum in the examined frequency interval of 200–4200 $cm^{-1}$.

The stretching H-H vibration band was decomposed to four Pseudo-Voit peaks with frequencies of 4147, 4154, 4158, and 4168 $cm^{-1}$ shown in Fig. 6. The frequency of 4158 $cm^{-1}$ of the most intense narrow peak with a width of 4.43 $cm^{-1}$ almost coincided with the frequency of 4156
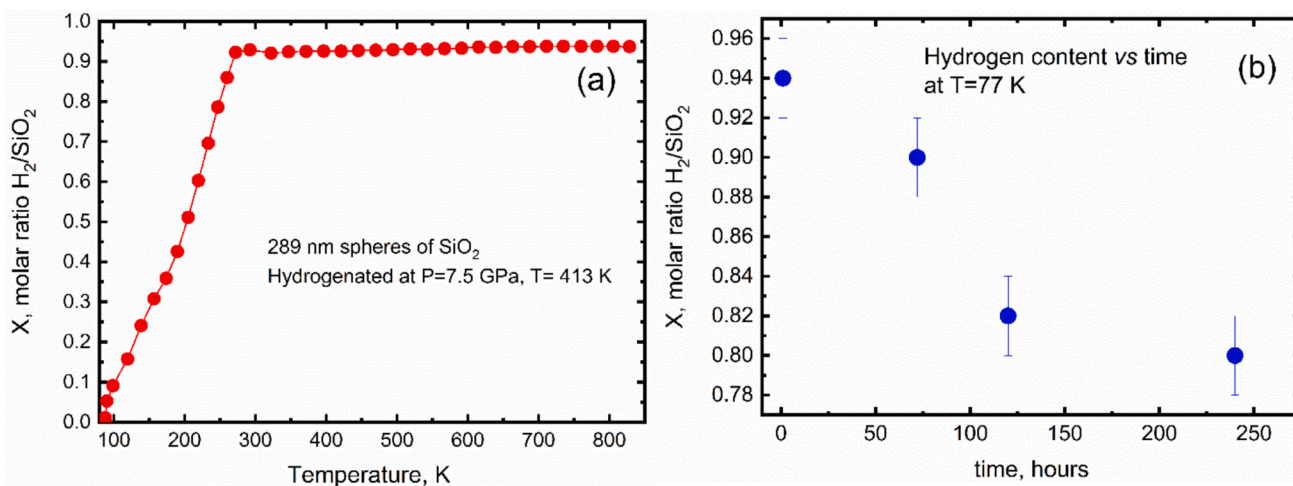


**Fig. 3.** Thermal desorption curve for the hollow silica nanospheres measured during the first 4 h after their hydrogenation at P = 7.5 GPa and T = 413 K (a) and the variation of the hydrogen content of these nanospheres depending on the time of their storage in liquid nitrogen at ambient pressure (b).
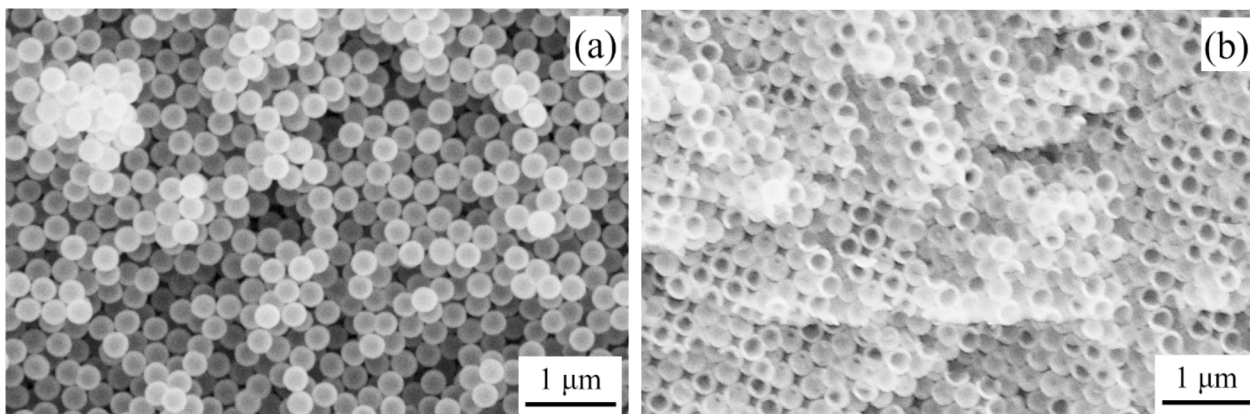
**Fig. 4.** SEM images of the initial sample (a) and the sample surface after hydrogenation at P = 7.5 GPa and T = 413 K and consequent annealing at temperatures up to 823 K in the pre-evacuated system (b).
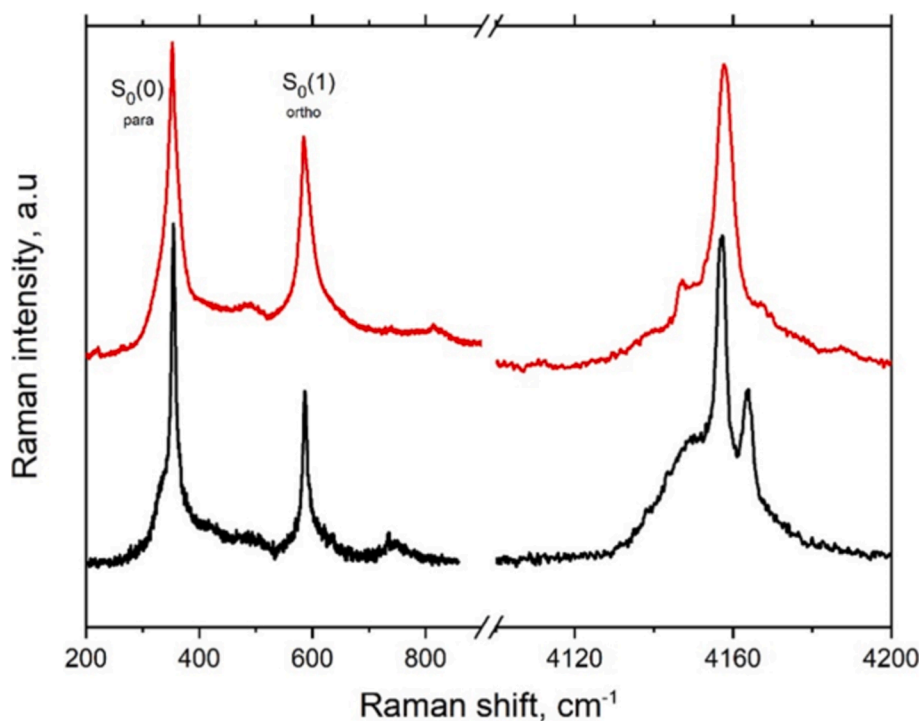


**Fig. 5.** Raman spectrum of the hollow silica nanospheres hydrogenated to X = 0.94 at P = 7.5 GPa and T = 413 K (upper spectrum, this data) and the hydrogenated OM1600 opal matrices (lower spectrum, data from Ref. 16). All spectra were collected at about 80 K and ambient pressure.

$cm^{-1}$ of the $Q_1(1)$ mode of a hydrogen gas [23]. Thus, it can be attributed to the hydrogen embedded into the cavity of the nanosphere.

The width and frequency of Raman scattering lines of $H_2$ molecules in a solid should differ from those of a free $H_2$ molecule due to their van der Waals interactions with neighboring atoms [24,25]. For example, a strong broadening of the H-H stretching line was previously observed for the hydrogen molecules dissolved in bulk silica glass [26,27] due to different Van der Waals forces in different interstitial voids. Thus, the band with a frequency of 4154 $cm^{-1}$ and a large width of 20.28 $cm^{-1}$ should correspond to the molecular hydrogen dissolved in the silica shell.

Assuming, as in Refs. [15,16], that the area $S_{peak}$ of each Raman $H_2$ peak is proportional to the amount X of molecular hydrogen in the corresponding state, the value of X can be estimated as:

$$X = (S_{peak}/S_{total}) \cdot X_{total} \tag{1}$$

where $X_{total}$ is the total hydrogen content determined by hot extraction.

According to the Raman band decomposition shown in Fig. 6, the ratio of the area of the $H_2$ narrow peak to the total area of the stretching band is $S_{4158}/S_{total} = 0.30$. The total amount of hydrogen dissolved in the sample and determined by hot extraction is X = 0.94. Thus, the cavities of the nanospheres contain about 0.28 mol of hydrogen gas per a mole of $SiO_2$, so the shells should contain X = 0.94–0.28 = 0.66 mol of hydrogen. The latter value correlates with the previously reported hydrogen solubility X = 0.6 ÷ 0.7 in bulk silica glass reached at the same hydrogen pressure [15]. This indicates a correct estimation of the hydrogen content of the cavities of nanospheres resulted from the Raman study in the present work.

Data on the size and thickness of the nanosphere shell obtained by electron microscopy allow one to estimate the volume of the nanosphere cavity. Using the volume of the cavity, the amount of the embedded hydrogen, and the equation of state of an ideal gas, the density and pressure of the embedded hydrogen gas were estimated. In Table 1, the
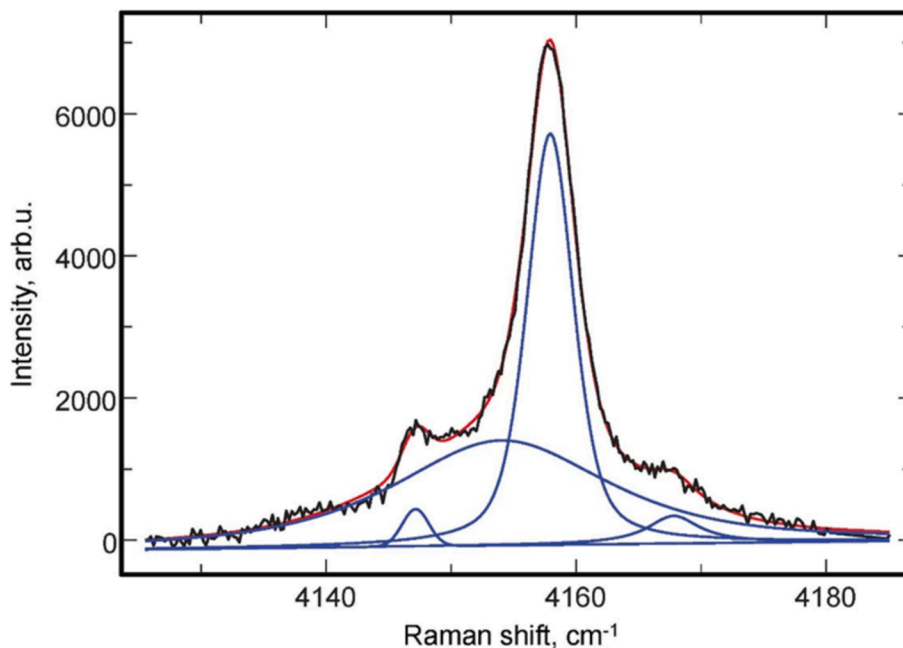
**Fig. 6.** Fitting of the $H_2$ phonon stretching band by the Pseudo-Voigt function.

**Table 1**

Hydrogen density in the SiO$_2$ nanospheres cavities estimated in this study and its density at normal pressure and at the critical point. The data marked with an asterisk were taken from the NIST database [28].

| Density of $H_2$, g/cm$^3$ | Pressure in the cavity, atm | Temperature, K |
|---|---|---|
| 0.016 | 52 | 80 |
| 0.031* | 12.79 | 33.14 |
| 0.000308* | 1 | 80 |

resulting value of the hydrogen density inside the nanosphere is compared with the hydrogen density at 1 atm and its density at the critical point.

As can be seen from Table 1, the density ρ≈0.016 g/cm$^3$ of gaseous hydrogen in the cavities is 52 times greater than the density of gaseous hydrogen at 1 atm and 80 K and, therefore, corresponds to a pressure of approximately 52 atm. Note also that the density of hydrogen in the cavities is comparable to its density ρ≈0.031 g/cm$^3$ at the critical point.

According to the criterion R > 5 × ΔR, where ΔR = 25 nm and R = 144.5 nm are the thickness of the sphere shell and its radius, the nanospheres can generally be attributed to thin-shell spheres [29,30]. In this case, the approximate external buckling pressure P that the silica nanosphere shell will withstand should be estimated by the classical formula for a thin-shell sphere taken from [31]:

$$P = \frac{2E \cdot \Delta R^2}{R^2 \cdot \sqrt{3 \cdot (1 - \nu^2)}} \qquad (2)$$

where E = 72 GPa is the Young's modulus of silica glass, ΔR and R are the thickness of the sphere shell and its radius, and ν = 0.17 is the Poisson's ratio. The value P = 3.45 GPa obtained in this way is higher than the external pressure of 1.5 GPa acting on the shell before the emergence of hydrogen. However, according to a lot of the experimental data, the collapsing of 80 % of the silicate glass microspheres arose at pressures 0.1–0.3 of the estimated one [32]. These results were explained by the presence of defects and roughness of the shell. Therefore, the nanospheres studied in this paper should collapse at P≈0.3–1 GPa. However, according to our experimental SEM data, the nanospheres had no noticeable deformation after the pressure loading up to 1.5 GPa and discharging. The absence of such destructions and

deformations in the nanospheres at much higher pressure can be explained by an increase in Young's modulus of silica glass by several times with a decrease in the dimensions of the shell from tens and hundreds of μm to tens of nm [33]. Alternatively, the absence of suitable amounts of defects and roughness on the shell of the silica glass nanospheres can also affect its stability.

The further processes of hydrogenation are schematically shown in Fig. 7. Due to the high value of $H_2$ diffusion coefficient D = 16 × 10$^{14}$ m$^2$/sec in the silica glass at T = 413 K [34], the hydrogen that appears in the high-pressure cell at 1.5 GPa should rapidly penetrate through the 25 nm thick shell of the nanosphere and fill the cavity, resulting in the equalization of the internal and external pressure acting on the shell. In this case, even at a maximum external pressure of 7.5 GPa outside the nanosphere, the value of internal hydrogen pressure is close to or identical to the external one. At this pressure and temperature of 413 K, the molar volume of hydrogen is V = 7.923 cm$^3$/mole [35], therefore its density is ρ = 0.25 g/cm$^3$. Assuming that the volume of the nanosphere cavity did not change after the sample was saturated with hydrogen and taking into account the amount of hydrogen dissolved in the shell, the total hydrogen content at P = 7.5 GPa and T = 413 K can be estimated as X = 5.14, where X is the $H_2$/SiO$_2$ molar ratio. Accordingly, the values of density ρ = 0.016 g/cm$^3$ and pressure P = 52 atm of hydrogen in the nanosphere cavity estimated in this work are probably residual values obtained when the external pressure was reduced from 7.5 GPa to normal pressure and the reverse diffusion of hydrogen through the shell occurred at liquid nitrogen temperature.

Also, it can be assumed that if the chemical composition and/or the thickness of the shell change, it is possible to slow down the reverse diffusion of hydrogen and, thus, increase the residual hydrogen density inside the cavity and the total hydrogen content in the nanosphere. Taking into account the above data on the Li$_2$O*6SiO$_2$-0.39H$_2$ solution, this effect can be achieved by adding lithium cations to the shell [36].

According to Chahine's rule, an increase in the specific surface area leads to a proportional increase in the maximum content of molecular hydrogen in a substance [37]. For example, a metal–organic framework with a specific surface area of 6245 m$^2$/g can contain up to 12 wt% molecular hydrogen [38], whereas carbon nanomaterials with a specific surface area of 3250 m$^2$/g dissolve up to 7 wt% $H_2$ [39]. A similar increase in the hydrogen content from X = 0.7 to X = 0.8 was also
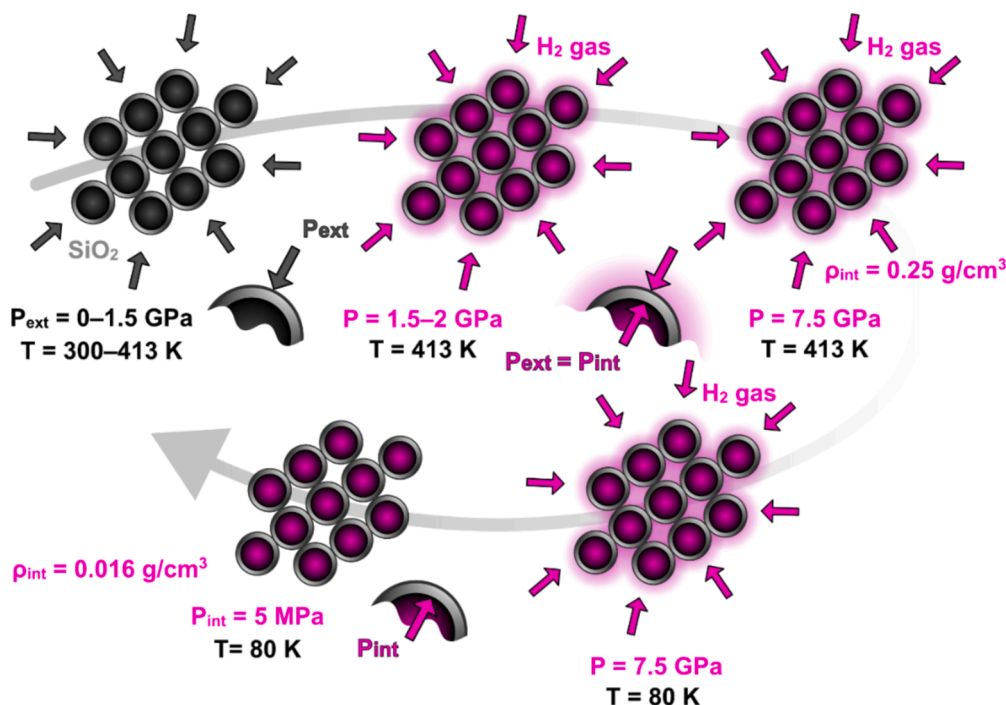
**Fig. 7.** Schematic representation of the hydrogenation of silica nanospheres. The black and purple arrows indicate quasi-hydrostatic and hydrogen pressure, respectively. (For interpretation of the references to colour in this figure legend, the reader is referred to the web version of this article.)

observed for $SiO_2$ after the transition of bulk silica glass with a minimum specific surface area [15] into OM1600 opals consisting of complex particles with a diameter of 1600 nm and a specific surface area of 630 $m^2/g$ [16]. This suggests that about X≈0.1 mol $H_2$ can be attributed to the gas phase or to $H_2$ molecules adsorbed on the surface of silica particles of OM1600 opals. The hydrogen content X = 0.28 achieved in our experiments in the cavities of the hollow silica nanospheres significantly exceeds the above value despite the relatively low specific surface area of 20 $m^2/g$. We believe that this fact indicates the importance of not only the specific surface area of a substance, the crystal structure, or the type of interatomic bonds but also its micro- and nanostructure, including the topology of the micro- and nano-voids available for hydrogen implementation, for the maximum hydrogen solubility in this hypothetic substance. If the micro-void has an "open" topology close to the cylinder, the hydrogen molecule in it can be held only by weak van der Waals forces near the void surface [40]. To escape from the spherical cavity, hydrogen should additionally overcome the shell with a diffusion activation barrier, which can be much higher than the surface one [15,34].

Various research groups have studied the possibility of using glass microspheres for hydrogen storage since 1981 [7,12,41–45]. The highest hydrogen content of 3.31 wt% was achieved at P = 10 atm and T = 473 K in the case of 50 µm glass microspheres doped with 2 wt% cobalt [46]. However, only the spheres with diameters greater than 5 µm were studied in the mentioned works. A considerable portion of these hollow spheres collapsed at pressures exceeding several thousand atmospheres due to the shell defects [31,47]. This limited the amount of hydrogen in the cavities inside the spheres and did not allow achieving significant hydrogen solubility in the shell material.

Thus, the use of the nanospheres with a diameter of 289 nm and a shell thickness of 25 nm in this study made it possible significantly to increase the hydrogenation pressure due to the greater strength of the silica spheres compared to spheres of a larger diameter. The hydrogenation at a higher pressure increased the hydrogen density in the cavities to a value close to the critical value required to form a uniform layer of condensed hydrogen on the inner surface of the spheres. As was said in the Introduction, this condition, as well as the amorphous state of the shell material and the small variation in the size of the spheres, are of

decisive importance for creating a center-symmetric shock wave and triggering a thermonuclear reaction.

It should also be noted that the hydrogenation at P = 7.5 GPa saturated the shell of the nanospheres with molecular hydrogen to X = 0.66. This hydrogen can be considered part of the fuel, since it is weakly bound to the shell and can quickly leave it at the rapid laser heating, thereby increasing the amount of hydrogen tending to the center of the cavity. Potentially, a higher hydrogen content can be achieved in silicate nanospheres at normal external pressure if the reverse hydrogen diffusion is minimized when the external pressure was reduced to the normal one.

## 4. Conclusions

In this work, opal matrix pellets consisting of hollow silica nanospheres with an outer diameter of 289 nm and a shell thickness of 25 nm were hydrogenated at high hydrogen pressure P = 7.5 GPa and temperature T = 413 K. The solubility X = 0.94 is the highest hydrogen content ever achieved in silicates, and a pressure of 7.5 GPa is the highest hydrogen pressure that was used for hydrogenation of hollow spheres for the first time. After keeping the sample in liquid nitrogen at normal pressure for three days, the hydrogen concentration decreased to X = 0.8 and then stopped changing. Despite a high value of hydrogen pressure, subsequent scanning electron microscopy showed that the hydrogenation did not change the shape of the nanospheres. Raman spectroscopy demonstrated that at T = 80 K and normal pressure, hydrogen molecules formed a gas in the cavities inside the spherical $SiO_2$ shells and a solid solution in those shells. The density of the $H_2$ gas inside the cavities estimated from the measured Raman spectra was about 0.016 $g/cm^3$, which is 52 times greater than its density at the same temperature and normal pressure.

Finally, the data of this work showed that the storage of molecular hydrogen in the hollow spheres with a submicron diameter and a shell thickness of tens of nm was more efficient than that in the substances containing "open" pores with a larger specific area or the hollow spheres with larger dimensions. The high density of the hydrogen gas of 0.016 $g/cm^3$ achieved in the sphere cavity can be useful for producing

perspective fuel targets in laser-initiated thermonuclear reactions.

## CRediT authorship contribution statement

**Vadim S. Efimchenko:** Writing – original draft, Methodology, Investigation, Funding acquisition, Conceptualization. **Konstantin P. Meletov:** Writing – review & editing, Resources, Methodology, Investigation, Formal analysis, Data curation. **Mariya A. Korotkova:** Visualization, Investigation, Formal analysis, Data curation. **Vladimir M. Masalov:** Resources, Methodology, Investigation. **Nadezhda S. Sukhinina:** Methodology, Investigation. **Gennadi A. Emel'chenko:** Resources, Methodology. **Radion I. Usmanov:** Formal analysis, Data curation.

## Declaration of competing interest

The authors declare the following financial interests/personal relationships which may be considered as potential competing interests: Vadim S. Efimchenko reports financial support was provided by Russian Science Foundation. If there are other authors, they declare that they have no known competing financial interests or personal relationships that could have appeared to influence the work reported in this paper.

## Acknowledgment

## Appendix A. Supplementary material

Supplementary data to this article can be found online at https://doi.org/10.1016/j.fuel.2024.134217.

## Data availability

No data was used for the research described in the article.

## References

[1] Drawer C, Lange J, Kaltschmitt M. Metal hydrides for hydrogen storage – identification and evaluation of stationary and transportation applications. J Energy Storage 2024;77:109988–10006. https://doi.org/10.1016/j.est.2023.109988.

[2] Ouyang L, Chen W, Liu J, Felderhoff M, Wang H, Zhu M. Enhancing the regeneration process of consumed $NaBH_4$ for hydrogen storage. Adv Energy Mater 2017;7:1700299–307. https://doi.org/10.1002/aenm.201700299.

[3] Zhu Y, Ouyang L, Zhong H, Liu J, Wang H, Shao H, et al. Closing the loop for hydrogen storage: facile regeneration of $NaBH_4$ from its hydrolytic product. Angew Chem Int Ed 2020;59:8623–9. https://doi.org/10.1002/anie.201915988.

[4] Chen Z, Kirlikovali KO, Idrees KB, Wasson MC, Farha OK. Porous materials for hydrogen storage. Chem 2022;8:693–716. https://doi.org/10.1016/j.chempr.2022.01.012.

[5] Lang C, Jia Y, Yan X, Ouyang L, Zhu M, Yao X. Molecular chemisorption: a new conceptual paradigm for hydrogen storage. Chem Synth 2022;2:1–13. https://doi.org/10.20517/cs.2021.15.

[6] Zhao YX, Gong MQ, Zhou Y, Dong XQ, Shen J. Thermodynamics analysis of hydrogen storage based on compressed gaseous hydrogen, liquid hydrogen and cryo-compressed hydrogen. Int J Hydrogen Energy 2019;44:16833–40. https://doi.org/10.1016/j.ijhydene.2019.04.207.

[7] Teitel RJ. Hydrogen Supply System. US Patent No. 4302217 1981, November 24.

[8] Kucheyev SO, Hamza AV. Condensed hydrogen for thermonuclear fusion. J Appl Phys 2010;108(091101–28):9. https://doi.org/10.1063/1.3489943.

[9] US Department of Energy Hydrogen. Targets for On-Board Hydrogen Storage Systems, http://www.eere.energy.gov/hydrogenandfuelcells/pdfs/freedomcar_targets_explanations.pdf; 2008 [accessed on December 20].

[10] Clark DS, Weber CR, Milovich JL, Salmonson JD, Kritcher AL, Haan SW, et al. Three-dimensional simulations of low foot and high foot implosion experiments on the national ignition facility. Phys Plasmas 2016;23:056302–19. https://doi.org/10.1063/1.4943527.

[11] Aleksandrova IV, Koresheva ER, Krokhin ON, Osipov IE. Cryogenic hydrogen fuel for controlled inertial confinement fusion (Formation of Reactor-Scale Cryogenic Targets). Phys Atom Nuclei 2016;79:1210–32. https://doi.org/10.1134/S1063778816070024.

[12] Schmitt M, Shelby JE, Hall MM. Preparation of hollow glass microspheres from sol–gel derived glass for application in hydrogen gas storage. J Non Cryst Solids 2006;352:626–31. https://doi.org/10.1016/j.jnoncrysol.2005.11.057.

[13] Masalov VM, Sukhinina NS, Khodos II, Zverkova II, Zhokhov AA, Emelchenko GA. Effect of heat treatment on the physical properties and morphology of hollow submicron $SiO_2$ particles. J Surf Investig 2021;15:1174–80. https://doi.org/10.1134/S1027451021060136.

[14] Sukhinina NS, Masalov VM, Fursova TN, Khodos II, Zverkova II, Zhokhov AA, et al. Heat-mediated transformation of pmma- $SiO_2$ core-shell particles into hollow $SiO_2$ particles. Crystals 2022;12:883–96. https://doi.org/10.3390/cryst12070883.

[15] Meletov KP, Efimchenko VS. Stability of hydrogenated silica glass and desorption kinetics of molecular hydrogen. Chem Phys Lett 2022;793:139477–81. https://doi.org/10.1016/j.cplett.2022.139477.

[16] Meletov KP, Efimchenko VS, Korotkova MA, Masalov VM, Sukhinina NS, Emel'chenko GA. Peculiarities of the absorption and desorption of hydrogen by opal matrices. Int J Hydrogen Energy 2023;48:14337–47. https://doi.org/10.1016/j.cplett.2022.139477.

[17] Sukhinina NS, Masalov VM, Khodos II, Zhokhov AA, Emelchenko GA. Evolution of the shell structure of hollow submicron $SiO_2$ particles during heat treatment. Bull Russ Acad Sci Phys 2023;87:1473–7. https://doi.org/10.3103/S1062873823703513.

[18] Khvostantsev LG, Slesarev VN, Brazhkin VV. Toroid type high-pressure device: history and prospects. High Pres Res 2004;24:371–83. https://doi.org/10.1080/08957950412331298761.

[19] Antonov VE, Bulychev BM, Fedotov VK, Kapustin DI, Kulakov VI, Sholin IA. $NH_3BH_3$ as an internal hydrogen source for high pressure experiments. Int J Hydrogen Energy 2017;42:22454–9. https://doi.org/10.1016/j.ijhydene.2017.03.12.

[20] Storozhenko PA, Svitsyn RA, Ketsko VA, Buryak AK, Ul'yanov AV. Ammineborane: synthesis and physicochemical characterization. Russ J Inorg Chem 2005;50:980–5.

[21] Nylén J, Sato T, Soignard E, Yarger JL, Stoyanov E, Häussermann U. Thermal decomposition of ammonia borane at high pressures. J Chem Phys 2009;131:104506–13. https://doi.org/10.1063/1.3230973.

[22] Bashkin IO, Antonov VE, Bazhenov AV, Bdikin IA, Borisenko DN. Thermally stable hydrogen compounds obtained under high pressure on the basis of carbon nanotubes and nanofibers. JETP Lett 2004;79:226–30. https://doi.org/10.1134/1.1753421.

[23] Antonov VE, Bashkin IO, Khasanov SS, Moravsky AP, Morozov YuG, YuM Shulga, Ossipyan YuA, Ponyatovsky EG. Magnetic ordering in hydrofullerite $C_{60}H_{24}$. J Alloys Compd 2002;330-332:365-8. doi: 10.1016/S0925-8388(01) 01534-1.

[24] Xu W, Liu X-D, Peña-Alvarez M, Jiang H-C, Dalladay-Simpson P, Coasne B, et al. High-pressure insertion of dense $h_2$ into a model zeolite. J Phys Chem C 2021;125:7511–7. https://doi.org/10.1021/acs.jpcc.1c02177.

[25] Strobel TA, Sloan ED, Koh CA. Raman spectroscopic studies of hydrogen clathrate hydrates. J Chem Phys 2009;130:014506. https://doi.org/10.1063/1.3046678.

[26] Efimchenko VS, Barkovskii NV, Fedotov VK, et al. High-pressure solid solutions of molecular hydrogen in amorphous magnesium silicates. J Alloys Comp 2019;770:229–35. https://doi.org/10.1016/j.jallcom.2018.08.111.

[27] Hartwig CM. Raman scattering from hydrogen and deuterium dissolved in silica as a function of pressure. J Appl Phys 1976;47:956–9. https://doi.org/10.1063/1.322686.

[28] NIST Chemistry WebBook, SRD 69, https://webbook.nist.gov/cgi/cbook.cgi?ID=C1333740; 2023.

[29] Kunieda H. Classical buckling load of spherical domes under uniform pressure. J Eng Mech 1992;118:1513–25. https://doi.org/10.1061/(ASCE)0733-9399(1992)118:8(1513).

[30] Morris NF. Shell stability: the long road from theory to practice. Eng Struct 1996;18:801–6. https://doi.org/10.1016/0141-0296(96)00009-0.

[31] Timoshenko SP, Goodier JN. Theory of Elasticity. 3rd edition. New York: McGraw-Hill; 1970.

[32] Yan D, Pezzulla M, Reis PM. Buckling of pressurized spherical shells containing a through-thickness defect. J Mech Phys Solids 2020;138:103923–42. https://doi.org/10.1016/j.jmps.2020.103923.

[33] An L, Zhang D, Zhang L. Effect of nanoparticle size on the mechanical properties of nanoparticle assemblies. Nanoscale 2019;11:9563–73. https://doi.org/10.1039/C9NR01082C.

[34] Shang L, Chou IM, La W, Burruss RC, Zhang Y. Determination of diffusion coefficients of hydrogen in fused silica between 296 and 523 k by Raman spectroscopy and application of fused silica capillaries in studying redox reactions. Geochem Cosmochim Acta 2009;73:5435–43. https://doi.org/10.1016/j.gca.2009.0.

[35] Tkacz M, Litwiniuk A. Useful equations of state of hydrogen and deuterium. J Alloys Compd 2002;330–332:89–92. https://doi.org/10.1016/S0925-8388(01)01488-8.

[36] Efimchenko VS, Korotkova MA, Meletov KP, Buchner S. Thermally stable concentrated solutions of molecular hydrogen in bulk lithium silicate glass. J Phys Chem C 2023;127:13538–46. https://doi.org/10.1021/acs.jpcc.3c02644.

[37] Bénard P, Chahine R. Storage of hydrogen by physisorption on carbon and nanostructured materials. Scr Mater 2007;56:803–8. https://doi.org/10.1016/j.scriptamat.2007.01.008.

[38] Gómez-Gualdrón DA, Wang TC, García-Holley P, Sawelewa RM, Argueta E, Snurr RQ, et al. Understanding volumetric and gravimetric hydrogen adsorption trade-off in metal–organic frameworks. ACS Appl Mater Interfaces 2017;9:33419–28. https://doi.org/10.1021/acsami.7b01190.

[39] Klechikov A, Mercier G, Sharifi T, Baburin IA, Seifert G, Talyzin AV. Hydrogen storage in high surface area graphene scaffolds. Chem Commun 2015;51:15280–3. https://doi.org/10.1039/C5CC05474E.

[40] De Kinder J, Bouwen A, Schoemaker D. Molecular hydrogen in porous vycor glass. PhysRevB 1995;52:15872–80. https://doi.org/10.1103/PhysRevB.52.15872.

[41] Kohli DK, Khardekr RK, Singh R, Gupta PK. Glass micro-container based hydrogen storage scheme. Int J Hydrogen Energy 2008;33:417–22. https://doi.org/10.1016/j.ijhydene.2007.07.044.

[42] Dalai S, Vijayalakshmi S, Shrivastava P, Sivam SP, Sharma P. Preparation and characterization of hollow glass microspheres (HGMs) for hydrogen storage using urea as a blowing agent. Microelectron Eng 2014;126:65–70. https://doi.org/10.1016/j.mee.2014.06.017.

[43] Dalai S, Vijayalakshmi S, Sharma P, Choo KY. Magnesium and iron loaded hollow glass microspheres (HGMs) for hydrogen storage. Int J Hydrogen Energy 2014;39:16451–8. https://doi.org/10.1016/j.ijhydene.2014.03.062.

[44] Dalai S, Savithri V, Shrivastava P, Param Sivam S, Sharma P. Fabrication of zinc-loaded hollow glass microspheres (HGMs) for hydrogen storage. Int J Energy Res 2015;39:717–26. https://doi.org/10.1002/er.3292.

[45] Li F, Zhou Y, Li B, Zhang Z. Permeation and photo-induced outgassing of deuterium in hollow glass microspheres doped with titanium. Int J Hydrogen Energy 2024;49:303–13. https://doi.org/10.1016/j.ijhydene.2023.08.114.

[46] Dalai S, Savithri V, Sharma P. Investigating the effect of cobalt loading on thermal conductivity and hydrogen storage capacity of hollow glass microspheres (HGMs). Mater Today Proc 2017;4:11608–16. https://doi.org/10.1016/j.matpr.2017.09.072.

[47] Duret B, Saudin A. Microspheres for on-board hydrogen storage. Int J Hydrogen Energy 1994;19:757–64. https://doi.org/10.1016/0360-3199(94)90240-2.